

Ergodic Magnetic Limiter for the TCABR

Elton C. da Silva, Iberê L. Caldas,
Instituto de Física, Universidade de São Paulo
C.P. 66318, 05315-970, São Paulo, SP, Brazil.

and Ricardo L. Viana
Departamento de Física, Universidade Federal do Paraná
C.P. 19081, 81531-990, Curitiba, PR, Brazil.

Received on 3 July, 2001

In this work it is considered the effect of an ergodic magnetic limiter on the plasma confined in the TCABR tokamak. The poloidal distribution of the limiter currents is determined taking into account the toroidal geometry of this tokamak. The plasma equilibrium field is analytically obtained by solving the Grad-Schlüter-Shafranov equation in polar toroidal coordinates. The perturbing limiter field is obtained as a vacuum field by solving the Laplace equation. Supposing the limiter action as a sequence of delta-function pulses, a symplectic map is derived by using a Hamiltonian formulation for the perturbed field line. Examples are given to illustrate the influence of this design on the topology of the perturbed field line structure.

I Introduction

The plasma confinement in tokamaks can be improved by creating a chaotic field line region which decreases the plasma-wall interaction [1, 2]. This chaotic region is created by suitably designed resonant magnetic windings which produce the overlapping of two or more chains of magnetic islands and, consequently, the magnetic surfaces destruction.

However, those windings have to be installed on the outside of the vacuum vessel, which is occupied by several diagnostics. This difficulty can be overcome by using a set of Ergodic Magnetic Limiters (EML) that are narrow slices of helical windings in the form of current rings, which are mounted along the toroidal direction.

The first conceptual and physical test of an EML scheme was carried out on the Texas Experimental Tokamak (TEXT) [3, 4]. Since then EMLs have been used in others tokamaks [5, 6] as a way of particle and heat control at the plasma edge [7].

Furthermore, it has recently been reported [8, 9] that runaway electron avalanches can be suppressed by the presence of radial diffusion. As the electrons with energies higher than the thermal energy are more sensitive to magnetic fluctuations it could be helpful to use EMLs in order to improve the radial diffusion of those electrons by producing a region of chaotic field lines.

A suitable design of an EML ring depends on the detailed knowledge of the toroidal geometry influence on the equilibrium field line configuration.

In this work, we present a symplectic map that describes the action of a set of EMLs for the toka-

mak TCABR.

This map allows us to generate Poincaré cross-sections faster in comparison with those obtained through numerical integration of field line equations.

In addition, the map we obtain can be regarded as a canonical transformation between angle-action variables derived from a Hamiltonian formulation. It is worth noting that this symplectic map embodies two important features: (i) it comes straightly from the expressions for the magnetic fields, and (ii) it preserves the main toroidal characteristics due to the confinement vessel geometry.

This map has recently been used to investigate anomalous field line diffusion and loss due to collision with the tokamak wall [10]; as well as the onset of chaos and bifurcations of magnetic axes [11].

Our paper is organized as follows. In section II, we outline the equilibrium and perturbing magnetic fields that are used in this work. In section III, the symplectic map for the set of EMLs is presented. In section IV, the influence of the EMLs on the magnetic surfaces for the TCABR tokamak parameters is discussed. Finally, in section V, our conclusions are summarized.

II Magnetic field configurations

The equilibrium magnetic field \mathbf{B}_0 is calculated from an ideal Magnetohydrodynamical (MHD) static equi-

librium given by the following set of equations:

$$\mathbf{J} \times \mathbf{B}_0 = \nabla p, \quad (1)$$

$$\nabla \times \mathbf{B}_0 = \mu_0 \mathbf{J}, \quad (2)$$

$$\nabla \cdot \mathbf{B}_0 = 0, \quad (3)$$

where p and \mathbf{J} are the equilibrium pressure and current density, respectively.

For an axisymmetric configuration, the above set of equations is reduced to the Grad-Schlüter-Shafranov equation, which describes the behavior of the poloidal magnetic flux Ψ .

To obtain Ψ , in terms of the polar toroidal coordinate system [12] $(r_t, \theta_t, \varphi_t)$, we assume [13] the following peaked current profile, commonly observed in tokamak discharges:

$$J_3(r_t) = \frac{I_p R'_0}{\pi a^2} (\gamma + 1) \left(1 - \frac{r_t^2}{a^2}\right)^\gamma, \quad (4)$$

in this expression, I_p and a are the plasma current and radius, respectively. The radial position of the magnetic axis in the cylindrical coordinate system is R'_0 and γ is a constant.

As a function of Ψ , the contravariant components of the equilibrium magnetic field \mathbf{B}_0 are:

$$B_0^1 = -\frac{1}{R'_0 r_t} \frac{\partial \Psi}{\partial \theta_t}, \quad (5)$$

$$B_0^2 = +\frac{1}{R'_0 r_t} \frac{\partial \Psi}{\partial r_t}, \quad (6)$$

$$B_0^3 = \frac{\mu_0 I_e}{2\pi R^2}, \quad (7)$$

where I_e is the external current that generates the toroidal magnetic field component and R is the radial coordinate in the cylindrical system.

At lowest order in $\frac{r_t}{R'_0}$, we obtain $\Psi \approx \Psi(r_t)$ and the following equilibrium magnetic field contravariant components:

$$B_0^1 = 0, \quad (8)$$

$$B_0^2 = B_a^2 \frac{a^2}{r_t^2} \left[1 - \left(1 - \frac{r_t^2}{a^2}\right)^{\gamma+1}\right], \quad (9)$$

$$B_0^3 = B_T^3 \frac{1}{1 - 2\frac{r_t}{R'_0} \cos(\theta_t)}. \quad (10)$$

Fig. 1 shows the contravariant components of the equilibrium magnetic field. We normalize the component B_0^2 to its value at $r_t = a$, $B_a^2 = \frac{\mu_0 I_p}{2\pi a^2}$, (Fig. 1a) and B_0^3 to its value at the magnetic axis, $B_T^3 = \frac{\mu_0 I_e}{2\pi R_0'^2}$, (Fig. 1b).

The corresponding safety factor q is:

$$\begin{aligned} q &= \frac{1}{2\pi} \int_0^{2\pi} \frac{B_0^3(r_t, \theta_t)}{B_0^2(r_t, \theta_t)} d\theta_t \\ &= \frac{q_c(r_t)}{\sqrt{1 - 4\frac{r_t^2}{R_0'^2}}}, \end{aligned} \quad (11)$$

with

$$q_c(r_t) = \frac{I_e}{I_p} \left(\frac{r_t}{R'_0}\right)^2 \frac{1}{1 - \left(1 - \frac{r_t^2}{a^2}\right)^{\gamma+1}}. \quad (12)$$

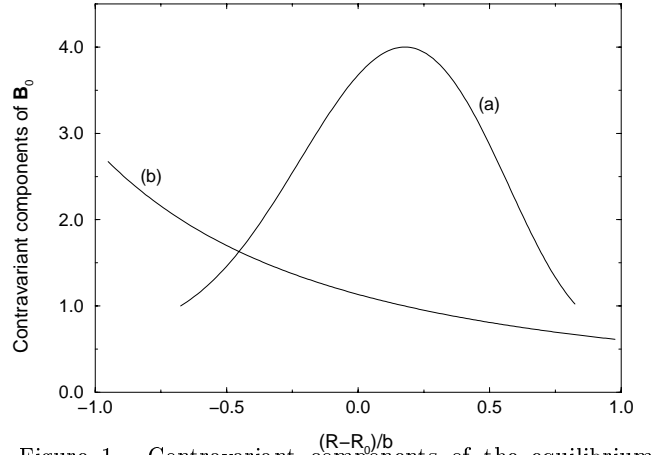


Figure 1. Contravariant components of the equilibrium magnetic field \mathbf{B}_0 . In (a), we show B_0^2 normalized to B_a^2 and in (b) we show B_0^3 normalized to B_T^3 .

This safety factor shows a parabolic profile with $q \approx 1.0$ at the magnetic axis and $q \approx 5.0$ at plasma edge (Fig. 2).

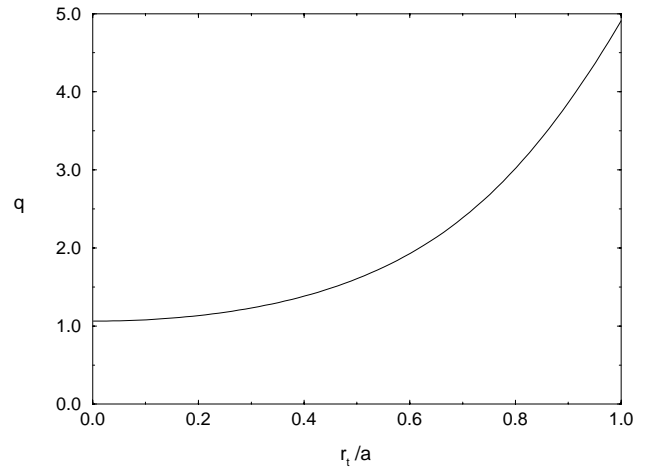


Figure 2. Radial profile of the safety factor. The radial coordinate r_t was normalized to the plasma radius a .

The perturbing magnetic field we consider in this paper is produced by a pair of helical windings installed on the external vacuum vessel surface. These conductors drive currents I_h in opposite directions. To produce an efficient resonant effect they must have the same pitch as the field lines in the rational magnetic surface with $q = \frac{m_0}{n_0}$ (m_0 and n_0 integers) we want

to disturb. The toroidal geometry makes the field line pitch nonuniform. In order to fit this nonuniformity we choose the following winding law for the current conductors:

$$u_t = m_0[\theta_t + \lambda \sin(\theta_t)] - n_0\varphi_t = \text{constant}. \quad (13)$$

The parameter λ is obtained by fitting this winding law to the equilibrium field line path in the rational surface with $q = \frac{m_0}{n_0}$. For $(m_0, n_0) = (5, 1)$ this parameter takes the value $\lambda = 0.59$ [13].

Therefore, we adopt the following expression for the helical current density:

$$\mathbf{J}_h = \frac{I_h}{R'_0 r_t} \delta(r_t - b_t) [\delta(u_t) - \delta(u_t - \pi)] \mathbf{e}_{u_t}, \quad (14)$$

that describes two current conductors located at the toroidal surface $r_t = b_t$, one of them driving a current I_h along the helix $u_t = 0$ and the other driving a current $-I_h$ along the helix $u_t = \pi$.

Basically, there are three different approaches to calculate the perturbing magnetic field. The first one is the direct determination of the magnetic field using the Biot-Savart law. The second one is to calculate straightly the vector potential for the magnetic field. The third one, which is the approach we choose, corresponds to the application of boundary conditions, derived from the helical current density, on a magnetic scalar potential Φ_M . The boundary conditions to be applied at the wall $r_t = b_t$ come from:

$$\mathbf{B}_1^{ext} - \mathbf{B}_1^{int} = -\mu_0 \int_{int}^{ext} d\mathbf{r}_n \times \mathbf{J}_h, \quad (15)$$

where $d\mathbf{r}_n$ is the differential vector perpendicular to the surface $r_t = b_t$. Here the perturbing magnetic field is a vacuum field: $\mathbf{B}_1 = \nabla \Phi_M$, where the magnetic scalar potential Φ_M satisfies the Laplace equation $\nabla^2 \Phi_M = 0$. In polar toroidal coordinate system, the Laplace equation reads [13]:

$$\begin{aligned} & \frac{1}{r_t} \frac{\partial}{\partial r_t} \left(r_t \frac{\partial \Phi_M}{\partial r_t} \right) + \frac{1}{r_t^2} \frac{\partial^2 \Phi_M}{\partial \theta_t^2} - \frac{r_t}{R'_0} \left\{ \cos(\theta_t) \left[2 \frac{\partial^2 \Phi_M}{\partial r_t^2} + \right. \right. \\ & \left. \left. + \frac{3}{r_t} \frac{\partial \Phi_M}{\partial r_t} \right] - \sin(\theta_t) \left[\frac{1}{r_t^2} \frac{\partial \Phi_M}{\partial \theta_t} + \frac{2}{r_t} \frac{\partial^2 \Phi_M}{\partial \theta_t \partial r_t} \right] \right\} + \\ & \left. + \frac{1}{R^2} \frac{\partial^2 \Phi_M}{\partial \varphi_t^2} = 0. \right. \end{aligned} \quad (16)$$

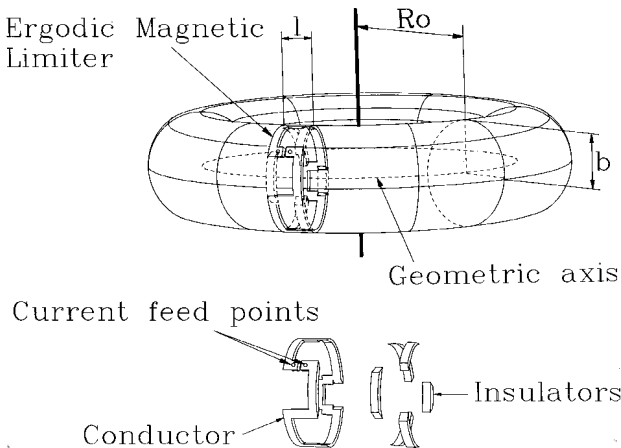


Figure 3. Schematic diagram of an Ergodic Magnetic Limiter.

As we have stated in the introduction, Ergodic Magnetic Limiters may be regarded as narrow slices of helical windings with lengths $l \ll 2\pi R_0$ (see Fig. 3), so

it is enough to take the lowest order solution of the Eq. (16) to model the EML perturbing magnetic field.

This lowest order solution of the Laplace equation is obtained by taking the real part of the following expression:

$$\begin{aligned} \Phi_M &= -\frac{\mu_0 I_h}{i\pi} \sum_{k=-m_0}^{m_0} J_k(m_0 \lambda) \left(\frac{r_t}{b_t} \right)^{m_0+k} \\ &\times e^{i[(m_0+k)\theta_t - n_0\varphi_t]}. \end{aligned} \quad (17)$$

Note that, due to the toroidal geometry effect, other modes besides the $(m_0, n_0) = (5, 1)$ are excited, whose amplitudes decay proportionally to Bessel functions of order k .

Therefore, from the above magnetic scalar potential Φ_M , and keeping in mind that only the lowest order solution is enough to model the EML action, the contravariant components of the perturbing magnetic field \mathbf{B}_1 are:

$$B_1^1 = \frac{\partial \Phi_M}{\partial r_t}, \quad (18)$$

$$B_1^2 = \frac{1}{r_t^2} \frac{\partial \Phi_M}{\partial \theta_t}, \quad (19)$$

$$B_1^3 = 0. \quad (20)$$

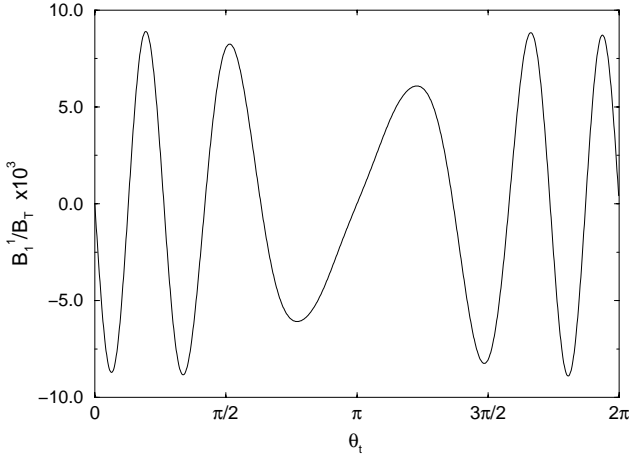


Figure 4. Contravariant component B_1^1 poloidal profile calculated at $\frac{r_t}{a} = 1$ and normalized to B_T . EML parameters: $(m_0, n_0) = (5, 1)$, $I_h = 3.2$ kA, $\lambda = 0.59$ and $N_r = 4$ rings symmetrically distributed along the toroidal direction.

Fig. 4 shows the poloidal profile of the perturbing magnetic field contravariant component B_1^1 calculated at plasma edge and normalized to B_T . Fig. 5 shows the radial profile of $\langle |B_1^1(r_t, \theta_t, \varphi_t)| \rangle_{\theta_t}$ normalized also to B_T . The symbol $\langle \cdot \rangle_{\theta_t}$ means an average taken along the poloidal direction, θ_t , keeping r_t and φ_t constant.

This perturbing contravariant component is chosen because it is most relevant to topological modifications of magnetic surfaces than the contravariant component B_1^2 .

To calculate these profiles we use the following EML parameters: $I_h = 3.2$ kA, $(m_0, n_0) = (5, 1)$, $N_r = 4$ and $\lambda = 0.59$.

From Fig. 5, we can see that the perturbing magnetic field strength decays rapidly with the radial distance from the plasma edge. Thus, the EML perturbing effect is important only close to the plasma edge, affecting less the plasma central region.

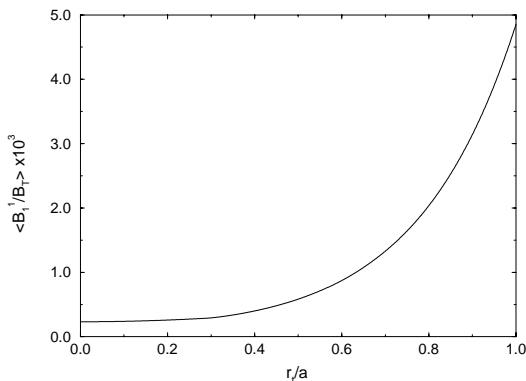


Figure 5. Radial profile of $\langle |B_1^1| \rangle_{\theta_t}$ normalized to B_T . EML parameters are the same as in Fig. 4.

Excluding marginal stability states, for which the plasma response would have to be taken into account, the total magnetic field is the superposition of the equilibrium and perturbing fields:

$$\mathbf{B} = \mathbf{B}_0 + \mathbf{B}_1. \quad (21)$$

III The symplectic map for the ergodic magnetic limiter

The perturbing magnetic field \mathbf{B}_1 we obtained can be described in terms of a vector potential \mathbf{A} as $\mathbf{B}_1 = \nabla \times \mathbf{A}$. This vector potential is related to the scalar potential Φ_M through the following expression: $\mathbf{A} = iR_0' \Phi_M \mathbf{e}^3$.

The trajectory of a magnetic field line is described by the equation:

$$\mathbf{B} \times d\mathbf{l} = 0, \quad (22)$$

where $d\mathbf{l}$ is an unitary displacement along the field line.

In terms of the polar toroidal coordinates, this field line equation reduces to a set of ordinary differential equations:

$$\frac{dr_t}{d\varphi_t} = -\frac{1}{r_t B_T} \left[1 - 2 \frac{r_t}{R_0'} \cos(\theta_t) \right] \frac{\partial}{\partial \theta_t} (\Psi + A_3), \quad (23)$$

$$\frac{d\theta_t}{d\varphi_t} = +\frac{1}{r_t B_T} \left[1 - 2 \frac{r_t}{R_0'} \cos(\theta_t) \right] \frac{\partial}{\partial r_t} (\Psi + A_3). \quad (24)$$

After transforming from the polar toroidal coordinate system $(r_t, \theta_t, \varphi_t)$ to a more suitable system of canonical coordinates $(\mathcal{J}, \vartheta, t)$, the above set of differential equations becomes the well known pair of Hamilton equations:

$$\frac{d\mathcal{J}}{dt} = -\frac{\partial H}{\partial \vartheta}, \quad (25)$$

$$\frac{d\vartheta}{dt} = \frac{\partial H}{\partial \mathcal{J}}. \quad (26)$$

These new angle-action variables are related to the polar toroidal coordinates in the following way [14]:

$$\mathcal{J} = \frac{1}{4} \left(1 - \sqrt{1 - 4 \frac{r_t^2}{R_0'^2}} \right), \quad (27)$$

$$\vartheta = 2 \arctan \left[\frac{1}{\Omega(r_t)} \left(\frac{\sin(\theta_t)}{1 + \cos(\theta_t)} \right) \right], \quad (28)$$

$$t = \varphi_t, \quad (29)$$

where

$$\Omega(r_t) = \frac{\sqrt{1 - 2 \frac{r_t}{R_0'}}}{\sqrt{1 + 2 \frac{r_t}{R_0'}}}, \quad (30)$$

in such a way that we have:

$$\begin{aligned} H(\mathcal{J}, \vartheta, t) &= H_0(\mathcal{J}) + H_1(\mathcal{J}, \vartheta, t) \\ &= \frac{1}{B_T R_0'^2} \Psi(\mathcal{J}) + \frac{1}{B_T R_0'^2} A_3(\mathcal{J}, \vartheta, t), \end{aligned} \quad (31)$$

as the Hamiltonian function.

Finally, if the ring length l is small enough, we can model the EML action as a sequence of impulsive perturbations centered at each ring position. This model allows us to adopt the EML Hamiltonian given below:

$$H_L = H_0(\mathcal{J}) + \frac{l}{R_0'} H_1(\mathcal{J}, \vartheta, t) \sum_{k=-\infty}^{\infty} \delta\left(t - k \frac{2\pi}{N_r}\right), \quad (32)$$

for N_r rings symmetrically distributed along the toroidal direction.

To the EML Hamiltonian (32) we can associate the following area-preserving mapping:

$$\mathcal{J}_{n+1} = \mathcal{J}_n + \epsilon f(\mathcal{J}_{n+1}, \vartheta_n, t_n), \quad (33)$$

$$\vartheta_{n+1} = \vartheta_n + \frac{2\pi}{N_r q(\mathcal{J}_{n+1})} + \epsilon g(\mathcal{J}_{n+1}, \vartheta_n, t_n), \quad (34)$$

$$t_{n+1} = t_n + \frac{2\pi}{N_r}, \quad (35)$$

with

$$f = -\frac{\partial H_1}{\partial \vartheta}, \quad g = \frac{\partial H_1}{\partial \mathcal{J}}, \quad (36)$$

$$\epsilon = 2 \frac{l}{R_0'} \frac{I_h}{I_e}. \quad (37)$$

When the perturbing current is turned off ($\epsilon = 0$) this map becomes a typical radial twist map, characteristic of integrable Hamiltonian systems.

IV Poincaré cross-section for the tcabr tokamak

This section is dedicated to present some results for the TCABR tokamak. Below, it is shown its typical parameters [15]:

TABLE 1. TCABR Parameters.

Parameter	Symbol	Value
Major radius	R_0	0.61 m
Minor radius ^a	b	0.22 m
Plasma radius	a	0.18 m
Toroidal magnetic field	B_T	1.2 T
Plasma current	I_p	70 kA
Safety factor at the edge	q	≈ 5
Electron thermal energy at the edge	kT_e	20 eV
Duration of the plasma discharge	τ	120 ms
Effective atomic number	Z_{eff}	≈ 4
Plasma current exponent	γ	3

^a The TCABR has rectangular cross-section, so b is the inscribed circumference radius in this cross-section.

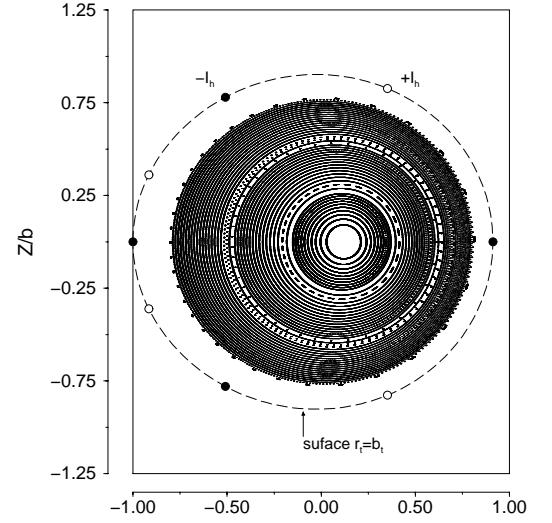


Figure 6. TCABR cross-section where it is shown some equilibrium magnetic surfaces and the symbols \bullet and \circ indicate the current conductor locations.

In Fig. 6, we see a TCABR vessel cross-section ($\varphi_t = 0$) and some equilibrium magnetic surfaces represented in terms of cylindrical coordinate system. Also it is possible to observe the surface $r_t = b_t$ where the nonuniformly distributed current segments are. These equilibrium surfaces have almost circular cross-sections and the Shafranov shift, due to the toroidal geometry, is clearly seen from the inner ones.

Fig. 7 shows the same equilibrium magnetic surfaces of Fig. 6 represented in terms of canonical coordinates.

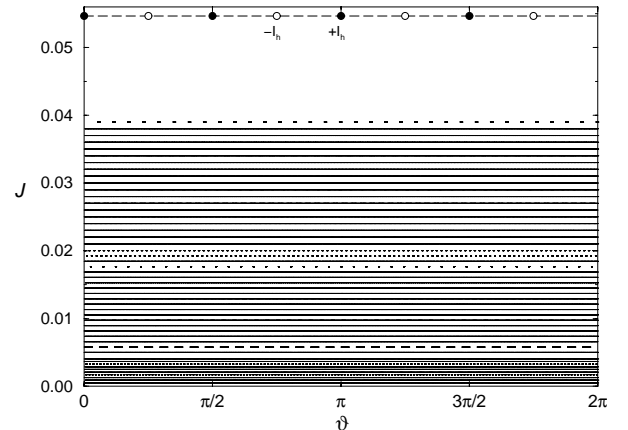


Figure 7. Equilibrium magnetic surfaces depicted in terms of canonical coordinates.

Although we have been doing most of our calculations in terms of both polar toroidal coordinate system (r_t, θ_t, φ_t) and canonical coordinate system ($\mathcal{J}, \vartheta, t$), it is more natural to present the results in terms of the

commonly used local polar coordinate system (r, θ, φ) . The relationship between this coordinate system and the cylindrical coordinate system is as follows:

$$R = R_0 - r \cos(\theta), \quad (38)$$

$$\Phi = \varphi, \quad (39)$$

$$Z = r \sin(\theta). \quad (40)$$

Fig. 8 shows the same surfaces that are shown in Fig. 7, but now in terms of the local polar coordinates.

From now on, we will use the local polar coordinate system to present the Poincaré cross-section we obtain for the TCABR tokamak.

When the perturbation is turned on, the magnetic surface topology changes notably and many island chains appear due to the resonant interaction between the equilibrium and the perturbing magnetic fields. There is a main chain of five magnetic islands around the equilibrium surface with $q = \frac{m_0}{n_0} = \frac{5}{1}$ and many others satellite island chains as well.

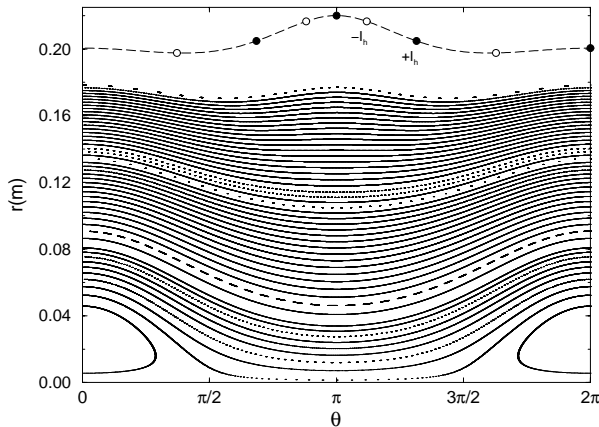


Figure 8. Surfaces shown in Fig. 7 now depicted in terms of the local polar coordinates ($\varphi = \text{constant}$).

Increasing the perturbing current, these island chains overlap and generate a sizable chaotic field line region. If the perturbing current is not large enough, this chaotic region does not reach the tokamak vessel wall because there still are some magnetic surfaces that are not destroyed between the vessel wall and the chaotic region. An example of this process can be seen in Fig. 9 where a Poincaré cross-section for the TCABR is shown corresponding to the following perturbing strength $\left\langle \frac{B^1(a)}{B_T} \right\rangle = 2.3 \times 10^{-3}$ ($I_h = 1.5$ kA, $(m_0, n_0) = (5, 1)$ and $\lambda = 0.59$).

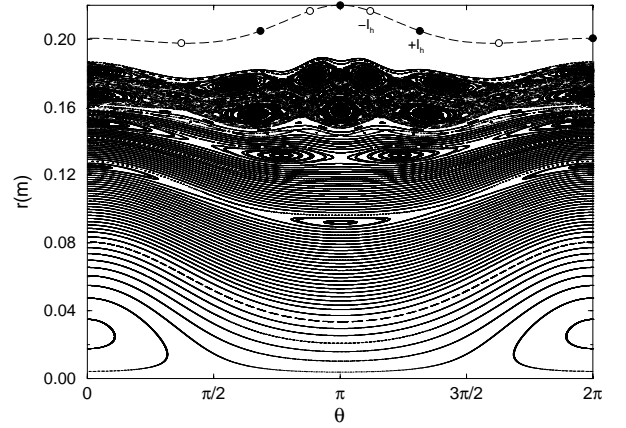


Figure 9. Poincaré cross-section for the TCABR tokamak. The EML parameters are: $I_h = 1.5$ kA, $(m_0, n_0) = (5, 1)$, $N_r = 4$ and $\lambda = 0.59$.

Increasing further the perturbing current, the last unperturbed surface which is located between the chaotic region and the vessel wall is destroyed. Consequently, a chaotic field line may reach the vessel wall after a finite number of turns around the confinement chamber. An example of this is shown in Fig. 10 where a current $I_h = 3.2$ kA produces the EML perturbing action with strength $\left\langle \frac{B^1(a)}{B_T} \right\rangle = 5.0 \times 10^{-3}$. The other parameters are the same as in Fig. 9.

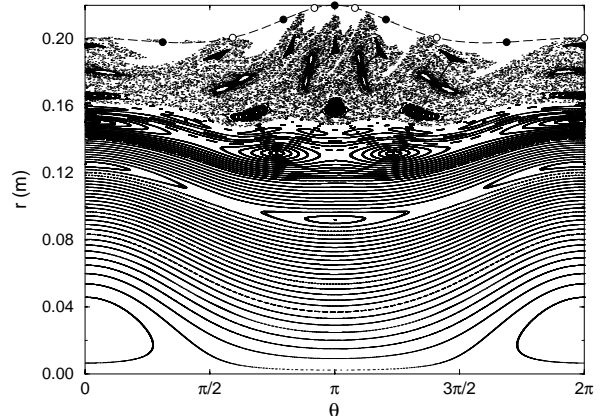


Figure 10. Poincaré cross-section for the TCABR tokamak. The EML parameters are: $I_h = 3.2$ kA, $(m_0, n_0) = (5, 1)$, $N_r = 4$ and $\lambda = 0.59$.

As an EML effectiveness estimation we calculate the average number of turns, $\langle n_c \rangle$, it takes for a chaotic field line to hit the vessel wall. We start with an ensemble of $N = 2000$ uniformly distributed initial points in the chaotic region and we calculate $\langle n_c \rangle$ as follows:

$$\langle n_c \rangle = \frac{1}{N} \sum_{i=1}^N n_{c_i}, \quad (41)$$

where n_{c_i} is the number of turns it takes for the i -th chaotic field line starting at the i -th initial point to reach the vessel wall.

With $\langle n_c \rangle$ we estimate an escape time required for an ionized impurity particle to hit the vessel wall. This escape time is given by $\tau_c = \frac{2\pi R_0 \langle n_c \rangle}{v_T}$ where $v_T = \sqrt{\frac{2k_B T}{m_p}}$ is the particle thermal velocity, $k_B T$ is the thermal energy and m_p is the particle mass. We choose the Beryllium mass ($m_p = 1.50 \times 10^{-26}$ kg) because its atomic number $Z = 4$ is almost equal to the TCABR plasma effective atomic number Z_{eff} .

Taking into account the perturbing current $I_h = 3.2$ kA, the escape time is $\tau_c \approx 28$ ms. This escape time is almost one fourth of the typical discharge duration $\tau = 120$ ms. Therefore, the EML can be activated during the plasma discharge. As we use a thermal velocity, this estimation may underevaluate possible effects due to the collisions between very fast particles (in the tail of the velocity distribution) and the tokamak wall.

V Conclusions

A conceptual design for a set of EML rings was proposed, which took into account toroidal geometry effects. The magnetic field of such a set of EML rings was calculated by using the same coordinate system as for the equilibrium field.

Considering the EML rings action as a sequence of impulsive perturbations and looking at the field line dynamic from a Hamiltonian point of view we obtained a symplectic map, in terms of angle-action variables, which embodies the following important characteristics:

(i) it results directly from the perturbing magnetic field expressions;

(ii) it has a control parameter λ introduced to match the actual equilibrium field line path and

(iii) it presents magnetic islands with different sizes and nonuniform poloidal distribution when they are represented in terms of local polar coordinates.

We applied this symplectic map for the TCABR tokamak conditions to estimate an impurity escape time. The escape time we estimated was almost one fourth of the discharge duration, so the EML rings

could be used effectively to improve the plasma confinement.

References

- [1] F. Karger and K. Lackner, Phys. Letters A **61** (6), 385 (1977).
- [2] W. Feneberg and G. H. Wolf, Nucl. Fusion **21**, 669 (1981).
- [3] N. Ohyabu, J. S. DeGrassie, *et al.*, J. Nucl. Mater. **121**, 363 (1984).
- [4] S. C. McCool, A. J. Wootton, *et al.*, Nucl. Fusion **29** (4), 547 (1989).
- [5] Y. Shen, M. Miyake, *et al.*, J. Nucl. Mater. **168**, 295 (1989).
- [6] A. Vannucci, I. C. Nascimento and I. L. Caldas, Plasma Phys. and Controlled Fusion **31**, 147 (1989).
- [7] N. Ohyabu, Nucl. Fusion **21**, 519 (1981).
- [8] R. Yoshino, T. Kondoh, *et al.*, Plas. Phys. Contr. Fusion **39**, 313 (1997).
- [9] P. Helander, L. G. Eriksson and F. Andersson, Phys. Plas. **7** (10), 4106 (2000).
- [10] E. C. da Silva, I. L. Caldas and R. L. Viana, Phys. Plasmas **8** (6), 2855 (2001).
- [11] E. C. da Silva, I. L. Caldas and R. L. Viana, "Bifurcations and Onset of Chaos on the Ergodic Magnetic Limiter Mapping", to be published in Chaos, Solitons & Fractals (2001).
- [12] M. Y. Kucinski, I. L. Caldas, *et al.*, J. Plas. Phys. **44**, 303 (1990).
- [13] E. C. da Silva, I. L. Caldas and R. L. Viana, IEEE Trans. on Plasma Science **29** (4), 617 (2001).
- [14] A. H. Boozer and A. B. Rechester, Phys. Fluids **21**, 682 (1978).
- [15] I. C. Nascimento *et al.*, "The TCABR Tokamak: Overview, Operational Regimes and Limits", in these proceedings.